ORIGINAL ARTICLE

Small capacitance self-shunted MoRe–Si(W)–MoRe junctions for SQUIDs applications

A. P. Shapovalov[1,2] · V. E. Shaternik[3] · O. G. Turutanov[4] · O. Yu. Suvorov[3] · A. A. Kalenyuk[3] · V. Yu. Lyakhno[4] ·
U. Yilmaz[5] · P. Febvre[5] · V. I. Shnyrkov[2]

Abstract

MoRe–Si(W)–MoRe planar Josephson junctions with a hybrid barrier layer made of amorphous silicon doped with tungsten at relatively high tungsten concentrations (~ 11%) are experimentally studied. Small intrinsic (natural) capacitance and shunting by tungsten nanoclusters give an advantage to MoRe–Si(W)–MoRe junctions against traditional superconductor–insulator–superconductor (SIS) planar junctions as candidates for innovative superconducting electronics. It is shown that the use of such junctions with a Si(W) barrier layer thickness of 15–30 nm can substantially enhance the sensitivity of both RF and DC SQUIDs.

Keywords Josephson contact · Tunnel junction · Barrier doping · Self-shunted junction · DC SQUID · RF SQUID

Introduction

Most of low-T_c DC and RF superconducting quantum interference devices (SQUIDs) operating as ultrasensitive detectors of magnetic flux are based on planar Nb–Al/Al$_2$O$_3$–Nb tunnel junctions which are superconductor–insulator–superconductor (SIS) trilayers. The large intrinsic capacitance of SIS structures restricts their range of operation in some applications. It is for instance at the origin of the limited bandwidth of SIS heterodyne receivers for submillimeter radio astronomy. To optimize the dynamic characteristics

of the contact, SIS junctions must be shunted by an external normal resistor of 1–2 Ω which is a common practice, but this deteriorates SQUID sensitivity. From the point of view of large-scale integration of Josephson devices and reduced number of operation steps for fabrication, a more promising way is to replace externally shunted junctions with self-shunted junctions. Currently, SQUIDs are widely used in medicine, geophysics, and novel physical experiments like in quantum informatics. Future advances in recently developed single microwave photon counter (Inomata et al. 2016; Koshino et al. 2016; Shnyrkov et al 2018) apparently requires improvement of both sensitivity and speed of the SQUID-based readout channel. The attempts of replacing SIS junctions by SNS junctions in which only the normal metal layer is responsible for weak coupling do not lead to a better SQUID sensitivity and cannot be considered as successful.

During the last years, a number of interesting results was achieved during the development of novel technologies for applications based on rapid single flux quantum (SFQ) digital circuits (Tolpygo et al. 2018) and on integrated circuits for Josephson voltage standards composed of several thousands of active elements per chip (Gudkov et al. 1988). The properties of Nb/αSi/Nb planar Josephson junctions with various degrees of doping of the amorphous silicon layer have been experimentally studied (Gudkov et al. 2012). By using tungsten as a dopant, self-shunted

✉ A. P. Shapovalov
  shapovalovap@gmail.com

1   V. N. Bakul Institute for Superhard Materials, National Academy of Sciences of Ukraine, Avtozavodskaya Str., 2, Kiev 04074, Ukraine

2   Kyiv Academic University, Academician Vernadsky Blvd., 36, Kiev 03142, Ukraine

3   G. V. Kurdyumov Institute for Metal Physics, National Academy of Sciences of Ukraine, Academician Vernadsky Blvd., 36, Kiev 03142, Ukraine

4   B. I. Verkin Institute for Low Temperature Physics and Engineering, National Academy of Sciences of Ukraine, Nauky Ave., 47, Kharkov 61103, Ukraine

5   IMEP-LAHC, Université Savoie Mont Blanc, 73376 Le Bourget du Lac Cedex, France

مدينة الملك عبدالعزيز
KACST للعلوم والتقنية

🙋 Springer

junctions were obtained with good characteristic voltage V_c of and low specific capacitance. Josephson junctions of SNS type are formed in the case of a fully degenerate αSi layer. The properties of such junctions are described by the classical resistive model. However, niobium is an active getter that may lead to negative consequences such as the deterioration of the barrier layer with time. Also, the niobium process requires high vacuum conditions during deposition and rather complicated micro- and nanostructures lithography procedures.

This work is aimed at developing a new fabrication process for more stable self-shunted MoRe–Si(W)–MoRe junctions with a low specific capacitance of 5–7 fF/μm² and characteristic voltages V_c in the range to enhance SQUID characteristics. The analysis of DC and RF SQUIDs sensitivities is carried out in the classic limit which is determined by the junction parameters and thermodynamic fluctuations.

Characterization of Josephson junction of various types

Josephson junctions are usually characterized by three channels of the current flow whose contribution is determined by the Josephson inductance $L_j = \Phi_0/2\pi I_c$, the normal resistance R_N and the capacitance C, where $\Phi_0 = h/2e$ is the quantum of magnetic flux, e is the electron charge, h is the Planck constant, and I_c is the junction critical current. Thus, the net current flowing through the junction is the sum of the superconducting current $I_c \sin \varphi$, the normal current V/R_N, and the displacement current $C\frac{dV}{dt}$. From the point of view of SQUID analysis, it is convenient to consider frequencies corresponding to these parameters. First, the plasma frequency of the junction is:

$$\omega_P = \frac{1}{\sqrt{L_j C}} = \sqrt{\frac{2eI_c}{\hbar C}} \sim \left(\frac{J_c}{C_S}\right)^{1/2}, \qquad (1)$$

where $J_c = I_c/S$ is the critical current density, S is the junction area, and $C_S = C/S$ is the specific capacitance of the junction. Second, the characteristic frequency

$$\omega = \frac{R_N}{L_j} = \frac{2\pi V_c}{\Phi_0}, \qquad (2)$$

which is proportional to an important junction parameter associated to the recombination of electrons in Cooper pairs: the critical voltage $V_c = I_c R_N$ that determines the upper limit of the ac Josephson effect. The third frequency is governed by the RC time constant of the equivalent junction circuit. It does not depend on the junction's area:

$$\omega_{RC} = \frac{1}{R_N C} = \frac{\omega_P^2}{\omega_c}. \qquad (3)$$

To analyze the junction dynamics at frequencies up to ω_c, it is suitable to use the dimensionless Stewart–McCumber parameter β_c responsible for the system damping:

$$\beta_c = \frac{2\pi R_N^2 I_c C}{\Phi_0}. \qquad (4)$$

Josephson tunnel junctions of superconductor–insulator–superconductor (SIS) type are fabricated (Yohannes 2012) on the base of niobium thin films separated by a thin dielectric barrier made of aluminum oxide. Nb–Al/Al₂O₃–Nb junctions show good reproducibility, thermocycling stability for a large range of critical current densities $J_c = 0.3 - 500 \ \mu A/\mu m^2$. The high specific capacitance C_S of such junctions of about 40–60 fF/μm² lowers the plasma frequency ω_p and increases the junction quality factor $\sim (\beta_c)^{1/2}$ making $\beta_c \gg 1$. To fulfill the requirement $\beta_c < 1$ necessary for the high sensitivity SQUIDs operation, SIS junctions are shunted by an additional external thin film resistor. In thin film junctions of superconductor–normal metal–superconductor (SNS) type, the condition $\beta_c < 1$ becomes valid automatically due to the small normal resistance and specific capacitance.

However, it is the small resistance of the SNS junctions that limits the range of applications of SNS junctions in many devices, including SQUIDs. The efforts to reduce the influence of the proximity effect and to raise the normal resistance by making additional dielectric barriers in multilayer structures like superconductor–insulator–normal metal–insulator–superconductor (SINIS) did not allow to obtain parameters better than the ones of SIS junctions (Yohannes 2012). Point contact superconductor–constriction–superconductor (ScS) (Likharev 1979) has a low capacitance, high values of plasma frequency ω_p and characteristic frequency ω_c. The excellent parameters of the ScS contacts enable their applicability in unique physical experiments. The most prominent example of ScS contacts is the atomic-size contact (Agraït et al. 2003). Unfortunately, their bad stability in time and to thermocycling seriously limits their practical usage.

In spite of the domination of SIS junctions in practical devices, researchers renewed their efforts (Kulikov et al. 1991; Gudkov et al. 2012; Baek et al. 2007) in recent years to enhance the characteristics determined by formulae (1)–(4) by exploiting structures with direct conductivity. The principal idea is well known and consists of the creation of a weak link made of normal metal with conductivity σ_n, small as compared to the normal-state conductivity of the superconducting banks σ_s. Practically, to limit the degradation of the superconducting order parameter in the

superconducting banks due to proximity effect, a stricter condition (Ivanov et al. 1981) should be fulfilled $\sigma_s/\xi_s \gg \sigma_n/\xi_n$, here ξ_s and ξ_n are the coherence lengths in the superconducting and the normal metals, respectively. Moreover, the characteristic size of the normal weak link should be small, $a \approx \xi_n$, to reach higher normal resistance of the contact and, therefore, better values of ω_c and V_c.

Experimental considerations

To prepare MoRe–Si(W)–MoRe planar junctions (Lacquaniti et al. 2016; Shaternik et al. 2017a, b), DC sputtering of MoRe and Si(W) was used in Ar flow at 0.1 Pa pressure. The thin films of MoRe and Si(W) were deposited through shadow masks onto polycrystalline-polished Al_2O_3 substrates. The MoRe target was a 0.5-mm-thick foil made of Mo–Re alloy (52 at% Mo and 48 at% Re). The composed target to deposit Si(W) thin films was fabricated on the base of a pure (99.99%) single-crystal silicon wafer. Both targets were soldered with indium to the magnetron surface to keep their temperature close to 300 K during the sputtering owing to the magnetron water cooling. To complete the composed target, 18–20 tungsten 10-mm-long wire cuts of 0.3 mm in diameter were placed onto the silicon wafer surface. The wire cuts were situated in the erosion zone of the silicon target perpendicular to the erosion ring and crossing it. During the magnetron sputtering of such composed target, the temperature of wires did not exceed 700 °C which was proved by dark red color of the wires glow. When Si and W were deposited simultaneously, the tungsten self-organized in nanoclusters within the hybrid Si(W) barrier layer of the junction trilayer structure. Further, structural analysis revealed amorphous state of both silicon and tungsten of the Si(W) barrier layer with this preparation technique.

The transmission electron microscopy (TEM) study of modeling Si(W) barrier layers witnesses the self-organized formation of tungsten nanoclusters inside the layer (Fig. 1). In 10-nm-thick Si(W) barrier layers deposited onto KCl substrates, tungsten aggregates in clusters of typical size approximately equal to the barrier thickness.

It is obvious from the Fig. 2 that different cluster arrangements, which depend on the tungsten content, correspond to different types of conductance of the composite structure. In the case I, the tungsten cluster creates a metallic short between MoRe layers yielding the direct metallic conductance. In the case II, when the cluster only slightly smaller than the Si layer thickness, the tunnel mechanism governs the charge transport. If the Si interspace between the W cluster and MoRe layers is very large to provide tunneling, like cases III and IV, there is no conductance of the structure at all. Also, a chain of smaller clusters distributed inside
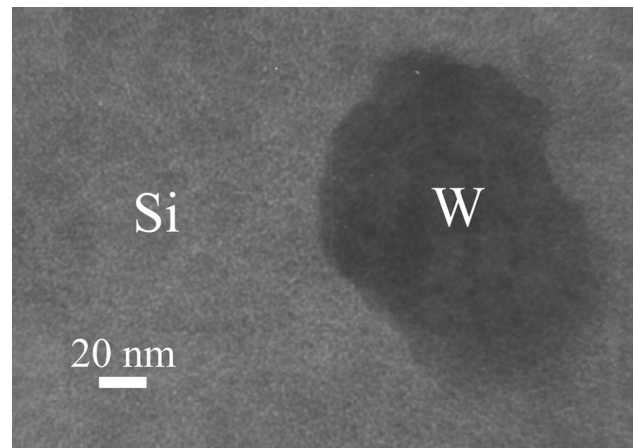

Fig. 1 TEM micrograph of modeling 100-nm-thick Si(W) barrier layer taken with JEOL JEM-2000FX
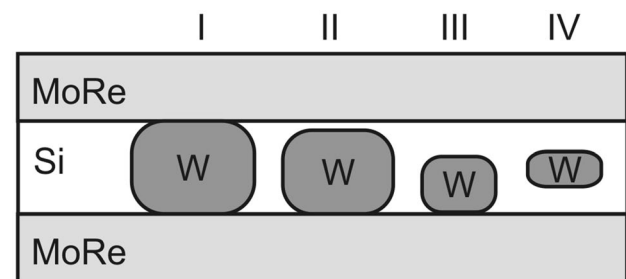

Fig. 2 Sketch of a MoRe–Si(W)–MoRe junction with silicon (Si) barrier layer-doped with tungsten (W) nanoclusters. Roman numerals denote possible nanocluster sizes and positions inside the Si layer which depend on the concentration of tungsten and the deposition rate

the silicon layer can be described in terms of one-dimensional percolation-resonant charge transport (see Shaternik et al. 2017a, b). Actually, the real heterostructures with the hybrid barrier layer show a mixture of different mechanisms depending on the W content and giving a flexibility in creating self-shunted Josephson junctions with required parameters.

The proposed barrier model is confirmed by atomic force microscopy (AFM) data for the Si(W) thin films (Fig. 3). In the non-contact frequency-modulation mode, AFM gives the phase contrast of the hybrid layer surface and quantitative data about the spacing between clusters.

It is well known that normal gradients of Van der Waals forces for metallic-phase tungsten and semiconductor matrix substantially differ. Consequently AFM measurements provide a "virtual landscape" (images of the clusters in the matrix) that displays information about the arrangement of the tungsten clusters in the silicon matrix.

It is follows from series of our experiments that the product $V_c = I_c R_N$ and, consequently, the characteristic
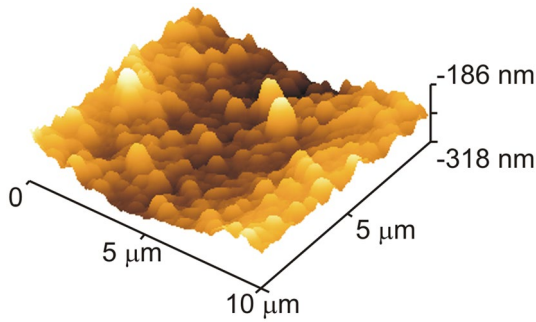
Fig. 3 Si(W) thin film surface image as a 3D landscape taken by AFM in non-contact mode. The substrate is Al_2O_3 ceramics
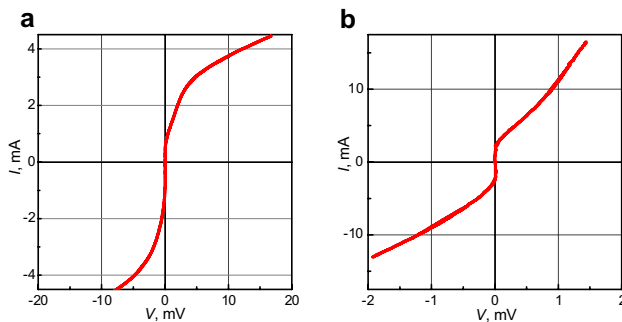

Fig. 4 Typical IVCs of MoRe/Si(W)/MoRe junctions 100×100 μm^2 in size with content of tungsten in barrier layers $n_W \approx 10$ at%; the temperature is 4.2 K, Si(W) barrier thicknesses $d = 15$ nm, critical currents $I_c = 1$ mA are equal. Deposition rates of Si(W) barrier layers are 1 nm/s and 0.3 nm/s, $R_N = 2$ Ω and 0.2 Ω, $V_c = I_c R_N = 2$ mV and 0.2 mV for (**a**, **b**), respectively

frequency ω_c of MoRe–Si(W)–MoRe junctions increase with the rise of the rate of simultaneous deposition of Si(W) thin film which forms the junction barrier layer. To obtain the mean value of the cluster size distribution in the barrier and V_c as a function of the deposition rate, the current–voltage characteristics (IVCs) of large area (100×100 μm^2) junctions were measured. Figure 4a, b show typical IVCs of MoRe–Si(W)–MoRe junctions with barrier layers of equal thickness $d = 15$ nm, but differing by the barrier deposition rate, the deposition regime and thicknesses of the top and bottom MoRe films were the same.

The values of the ω_c, ω_p, ω_{RC} frequencies, specific capacitance C_S, and normal resistance R_N of MoRe/Si(W)/MoRe junctions are in good agreement with results (Gudkov et al. 2012) obtained for Nb/Si(W)/Nb junctions. To our opinion, the replacement of Nb by MoRe will increase the stability of RF and DC SQUIDS because of some Nb disadvantages: (a) Nb behaves as an active getter during deposition and further junction exploitation and (b) Nb can grow in whisker crystals spoiling junction barriers. However, we have no

systematic experimental evidence for the junction lifetime comparison at the moment.

DC SQUID with MoRe–Si(W)–MoRe junctions

The DC SQUID consists of two Josephson junctions in a superconducting loop of inductance L. Each SIS junction has a critical current I_c, a capacitance C and is shunted by a linear resistance R_N. The maximum zero-voltage current I_{max} that can be driven through the SQUID in the absence of applied magnetic flux is $2I_c$.

As the external flux Φ_e is varied, $I_{max}(\Phi_e)$ will decrease, reach a minimum, and then return back to its maximum value with the period equal to the superconducting flux quantum Φ_0. So Φ_e is usually normalized to Φ_0: $\varphi_e = {2\pi\Phi_e}/{\Phi_0}$. The critical current modulation depth ${\Delta I_{max}(\varphi_e)}/{2I_c}$ is a function of the DC SQUID parameter

$$\beta = \frac{2LI_c}{\Phi_0}. \tag{5}$$

Modulation depth is about 50% (Barone and Paternò 1982) if $\beta = 1$ and is $\Delta I_{max} \approx {\Phi_0}/{L}$ for devices with the parameter $\beta \gg 1$. Then the maximum voltage variation ΔV with the DC SQUID biased at some constant current will be

$$\Delta V \approx \Delta I_{max} \frac{R_N}{2} \approx \frac{\Phi_0}{L} \frac{R_N}{2}. \tag{6}$$

Assuming roughly triangular $V(\varphi_e)$ characteristic, this leads to the flux–voltage transfer function proportional to shunting resistance of the two shunt resistors in parallel

$$\frac{\partial V}{\partial \varphi_s} \approx \frac{\Delta V}{\left(\Phi_0/2\right)} \approx \frac{R_N}{2L}. \tag{7}$$

Let us assume that, for practical devices, condition $\beta_c < 1$ (Eq. 4) is valid. Then the thermal voltage noise across the DC SQUID is of the order of Johnson noise of the two shunt resistors connected in parallel and has the voltage spectral density

$$S_V = 4k_B T\left(R_N/2\right), \tag{8}$$

where k_B is the Boltzmann constant, T is the physical temperature.

Then the spectral density of the thermal flux noise in the DC SQUID reads as

$$S_\Phi = S_V \left(\frac{\partial V}{\partial \varphi_e}\right)^{-2} \approx \frac{8k_B TL^2}{R_N} = h\left(\frac{2k_B TL}{eR_N I_c}\right), \tag{9}$$

when the optimum condition (Tesche and Clarke 1977, 1979) $\beta = 1$ is valid, i.e. $2LI_c = {h}/{2e}$. So, for the fluctuation-limited energy resolution (sensitivity) of the DC SQUID we will get

$$\delta E = \frac{S_\Phi}{2L} = \alpha \cdot h \frac{k_B T}{e R_N I_c} = \alpha \cdot \frac{k_B T}{\pi \omega_c}. \tag{10}$$

As it follows from numerical calculations (Tesche and Clarke 1977, 1979) and experimental results, the factor $\alpha \sim \pi$ is taken for the ratio of the thermal energy to the Josephson coupling energy $\gamma = \frac{2\pi k_B T}{I_c \Phi_0} = 0.05$. Expression (10) demonstrates the important role of the increase of the characteristic frequency ω_c (Eq. (2)) from the point of view of DC SQUID design.

MoRe–Si(W)–MoRe junctions with Si(W) barrier thickness of $d = 20 - 30$ nm being self-shunted by the tungsten nanoclusters, exhibit much smaller specific capacitance C_S than for traditional SIS structures, so that the condition $\beta_c < 1$ is fulfilled for the R_N values which are higher by a factor of 3–4 than the corresponding SIS shunt resistances. In turn, keeping the condition $\beta = 1$ results in a proportional increase of the characteristic frequency $\omega_c \sim I_c R_N$. For MoRe–Si(W)–MoRe junctions with $d \approx 30$ nm, the value of $I_c R_N$ ranges from 20 to 200 μV. This range is determined by different states of tungsten nanoclusters in the silicon matrix. If $k_B T << e I_c R_N$; $\pi \omega_c$, the intrinsic sensitivity of DC SQUIDs with MoRe–Si(W)–MoRe junctions in the white noise region is limited by quantum fluctuations reaching the quantum limit (Ketchen 1981; Tesche and Clarke 1979)

$$\delta \varepsilon = \frac{\left(\delta \Phi_{\min} \right)^2}{2L} \geq \frac{\hbar}{2}, \tag{11}$$

where $\delta \Phi_{\min}$ is the resolution of the DC SQUID by magnetic field in a 1 Hz frequency band.

However, in some applications (e.g., microwave single-photon counters (Inomata et al. 2016; Shnyrkov et al. 2018) and for the readout for superconducting qubit state (Clarke and Wilhelm 2008) the Josephson generation at the operation point of the DC SQUID associated with the wideband Nyquist noise of shunt resistors may lead to an increase of "dark" counts, and destruction of quantum superposition states, and even to mixing of the discrete energy spectrum level of the device under measurement.

To reduce the SQUID back action at a measured quantum system, a magnetometer can be used that is based on an RF SQUID in non-hysteretic regime with parameter $\beta_L = \frac{2\pi L I_c}{\Phi_0} < 1$, where I_c is the Josephson junction critical current, L is the geometric interferometer inductance. The absence of phase jumps and corresponding hysteresis losses which are inherent to the hysteretic regime

with $\beta_L > 1$ make the non-hysteretic RF SQUID to be almost ideal parametric frequency upward shifter (Shnyrkov et al. 1980; Dmitrenko et al. 1982). Generally, the transmission frequency band (operation rate) and the sensitivity of RF SQUIDs increase with the pump frequency ω. However, the frequency properties of Josephson junctions greatly influence the SQUID operation and may violate the conditions of the "ideality" with the increase of the pump frequency. The use of self-shunted Josephson junctions with low specific capacitance and high characteristic frequencies enables one to build a measuring system on the base of RF SQUID with pump frequency $\omega/2\pi = 0.5 - 1$ GHz, while the introduction of ultralow power consumption HEMT amplifiers (Korolev et al. 2011, 2015) combined with RF SQUIDs makes it possible to place the amplifier at 10–20 mK temperature stage thus reducing noises and back action at the quantum system under measurement (Shnyrkov et al. 2015).

Conclusion

The characteristic voltage $V_c = I_c R_N$ plays a crucial role in determining the classical noise, performance, and sensitivity of DC SQUIDs. We present a magnetron sputtering technology for producing small capacitance self-shunted MoRe–Si(W)–MoRe junctions with $I_c R_N$ products of 20–200 μV for SQUIDs applications.

The key points are as it follows. First, it is a self-shunted junction. The growth of tungsten nanoclusters in the silicon matrix provides high-resistance shunting with $R_N = 10 - 50$ Ω directly in the barrier layer of the Josephson junction. Second, such inner shunting by tungsten nanoclusters makes the physical properties of the junctions close the SNS junction model, so that the self-shunted MoRe–Si(W)–MoRe junctions demonstrate high enough critical current densities even at thicknesses of the barrier layer of 20–30 nm. In turn, large thickness of the barrier layer as compared to 2 nm which is typical for SIS junctions results in a specific capacitance, an order of magnitude smaller while keeping $\beta_c < 1$ for realistic values of the critical currents corresponding to $\beta_L \approx 1$. As a result, the thermal contribution to the intrinsic energy sensitivity of the DC SQUIDs at temperature 4.2 K can reach $(3 - 4)h$.

References

Agraït N, Yeyati AL, van Ruitenbeek JM (2003) Quantum properties of atomic-sized conductors. Phys Rep 377:81–279. https://doi.org/10.1016/S0370-1573(02)00633-6

Baek B, Dresselhaus PD, Benz SP (2007) Thermal stability of Nb/a–Nb$_x$Si$_{1-x}$/Nb Josephson junctions. Phys Rev B 75:054514–1–054514-6. https://doi.org/10.1103/PhysRevB.75.054514

Barone A, Paternò G (1982) Physics and applications of the Josephson effect. Wiley, New York

Clarke J, Wilhelm FK (2008) Superconducting quantum bits. Nature 453:1031–1042. https://doi.org/10.1038/nature07128

Dmitrenko IM, Tsoi GM, Shnyrkov VI, Kartsovnik VV (1982) RF SQUID in the nonhysteretic regime with k^{2}Ql>1. J Low Temp Phys 49:417–433. https://doi.org/10.1007/bf00681894

Gudkov AL, Kupriyanov MY, Likharev KK (1988) Properties of Josephson junctions with amorphous-silicon interlayers. Sov Phys JETP-USSR 67:1478–1485

Gudkov AL, Kupriyanov MY, Samus' AN (2012) Properties of planar Nb/α-Si/Nb Josephson junctions with various degrees of doping of the α-Si layer. J Exp Theor Phys 114:818–829. https://doi.org/10.1134/S1063776112030144

Inomata K, Lin Zh, Koshino K, Oliver WD, Tsai J-S, Ts Y, Nakamura Y (2016) Single microwave-photon detector using an artificial Λ-type three-level system. Nat Commun 7:12303–1–12303-7. https://doi.org/10.1038/ncomms12303

Ivanov ZG, Kupriyanov MYu, Likharev KK, Meriakri SV, Snigirev OV (1981) Boundary conditions for the Eilenberger and Usadel equations and properties of "dirty" SNS sandwiches. Sov J Low Temp Phys 7:274–281

Ketchen M (1981) DC SQUIDs 1980: the state of the art. IEEE T on Magn 17:387–394. https://doi.org/10.1109/TMAG.1981.1061180

Korolev AM, Shnyrkov VI, Shulga VM (2011) Ultra-high frequency ultra-low dc power consumption HEMT amplifier for quantum measurements in millikelvin temperature range. Rev Sci Instr 82:016101–1–016101-3. https://doi.org/10.1063/1.3518974

Korolev AM, Shulga VM, Turutanov OG, Shnyrkov VI (2015) A wideband radio-frequency amplifier for investigations at temperatures from 300 to 0.1 K. Instrum Exp Tech 58:478–482. https://doi.org/10.1134/s0020441215030227

Koshino K, Inomata K, Lin ZH, Nakamura Y, Yamamoto TS (2015) Theory of microwave single-photon detection using an impedance-matched Λ system. Phys Rev A 91:043805–1–043805-9. https://doi.org/10.1103/PhysRevA.91.043805

Koshino K, Lin ZH, Inomata K, Yamamoto TS, Nakamura Y (2016) Dressed-state engineering for continuous detection of itinerant microwave photons. Phys Rev A 93:023824–1–023824-8. https://doi.org/10.1103/PhysRevA.93.023824

Kulikov VA, Matveets LV, Gudkov AL, Laptev VN, Makhov VI (1991) A MM-wave radiometer with planar Nb/a-Si/Nb Josephson junction. IEEE T Magn 27:2468–2471. https://doi.org/10.1109/20.133719

Lacquaniti V, Cassiago C, De Leo N, Fretto M, Sosso A, Febvre P, Shaternik V, Shapovalov A, Suvorov O, Belogolovskii M, Seidel P (2016) Analysis of internally shunted Josephson junctions. IEEE T Appl Supercon 26:1100505–1–1100505-5. https://doi.org/10.1109/TASC.2016.2535141

Likharev KK (1979) Superconducting weak links. Rev Mod Phys 51:101–159. https://doi.org/10.1103/RevModPhys.51.101

Shaternik VE, Shapovalov AP, Prikhna TA, Suvorov OY, Skorik MA, Bondarchuk VI, Moshchil VE (2017a) Charge transport in hybrid tunnel superconductor-quantum dot-superconductor junctions. IEEE T Appl Supercon 27:1800507–1–1800507-7. https://doi.org/10.1109/TASC.2016.2636255

Shaternik VE, Shapovalov AP, Suvorov OY (2017b) Charge transport in superconducting MoRe–Si(W)–MoRe heterostructures with hybrid semiconductor barrier containing metal nanoclusters. Low Temp Phys 43:877–881. https://doi.org/10.1063/1.4995640

Shnyrkov VI, Khlus VA, Tsoi GM (1980) On quantum interference in a superconducting ring closed by a weak link. J Low Temp Phys 39:477–496. https://doi.org/10.1007/bf00114891

Shnyrkov VI, Korolev AM, Turutanov OG, Shulga VM, Lyakhno VY, Serebrovsky VV (2015) Isolation of a Josephson qubit from the electromagnetic environment. Low Temp Phys 41:867–873. https://doi.org/10.1063/1.4935839

Shnyrkov VI, Yangcao W, Soroka AA, Turutanov OG, Lyakhno VYu (2018) Frequency-tuned microwave photon counter based on a superconductive quantum interferometer. Low Temp Phys 44:213–220. https://doi.org/10.1063/1.5024538

Tesche CD, Clarke J (1977) dc SQUID: noise and optimization. J Low Temp Phys 29:301–331. https://doi.org/10.1007/BF00655097

Tesche CD, Clarke J (1979) dc SQUID: current noise. J Low Temp Phys 37:397–403. https://doi.org/10.1007/BF00119197

Tolpygo SK, Bolkhovsky V, Oates DE, Rastogi R, Zarr S, Day AL, Weir TJ, Wynn A, Johnson LM (2018) Superconductor electronics fabrication process with MoNx kinetic inductors and self-shunted josephson junctions. IEEE T Appl Supercond 28:1–12. https://doi.org/10.1109/TASC.2018.2809442

Yohannes DT (2012) Niobium integrated circuit fabrication, process #03–10–45, Design rules, Revision #25, 12/12/2012. Hypres, Inc. https://www.hypres.com/wp-content/uploads/2010/11/DesignRules-4.pdf. Accessed 10 Jan 2020

Springer